

## Onset conditions for equatorial spread $F$ determined during EQUIS II

D. L. Hysell,<sup>1</sup> M. F. Larsen,<sup>2</sup> C. M. Swenson,<sup>3</sup> A. Barjatya,<sup>3</sup> T. F. Wheeler,<sup>4</sup>  
M. F. Sarango,<sup>5</sup> R. F. Woodman,<sup>5</sup> and J. L. Chau<sup>5</sup>

Received 23 September 2005; revised 3 November 2005; accepted 14 November 2005; published 22 December 2005.

[1] An investigation into the dynamics and layer structure of the postsunset ionosphere prior to the onset of equatorial spread  $F$  (ESF) took place during the NASA EQUIS II campaign on Kwajalein Atoll on August 7 and 15, 2004. On both nights, an instrumented rocket measured plasma number density and vector electric fields to an apogee of about 450 km. Two chemical release rockets were launched both nights to measure lower thermospheric wind profiles. The Altair UHF/VHF radar was used to monitor coherent and incoherent scatter. In both experiments, strong plasma shear flow was detected. Periodic, patchy bottom-type scattering layers were observed in the westward-drifting plasma below the shear nodes. The large-scale plasma depletions that formed later during ESF reproduced the periodic structure of the original, precursor layers. The layers were therefore predictive of the ESF that followed. We surmise that collisional shear instabilities may have given rise to large-scale plasma waves that were highlighted by the bottom-type layer structure and that preconditioned the postsunset ionosphere for ESF. **Citation:** Hysell, D. L., M. F. Larsen, C. M. Swenson, A. Barjatya, T. F. Wheeler, M. F. Sarango, R. F. Woodman, and J. L. Chau (2005), Onset conditions for equatorial spread  $F$  determined during EQUIS II, *Geophys. Res. Lett.*, 32, L24104, doi:10.1029/2005GL024743.

### 1. Background

[2] We describe a NASA sounding rocket investigation into the dynamics of the postsunset equatorial  $F$  region ionosphere and the role of thin “bottom-type” coherent scattering layers that form at sunset. Coherent scatter from these layers is thought to be a precursor to fully developed equatorial spread  $F$  (ESF) [Woodman and La Hoz, 1976]. The enigmatic layers exhibit no vertical development and reside in the valley region, below the shear node, where the plasma flow is westward and retrograde (opposite the wind direction) [Hysell and Burcham, 1998]. Kudeki and Bhattacharyya [1999] argued that plasma irregularities in the layers are generated by wind-driven interchange instabilities operating near the equatorial evening vortex. Hysell *et al.* [2004] found the layers to be patchy, suggesting the presence of large-scale waves stable and

unstable to horizontal wind-driven instabilities in opposite phases. Hysell and Kudeki [2004] then hypothesized that the shear flow in the bottomside may destabilize the bottomside, generating the large-scale waves and preconditioning the ionosphere for ESF.

[3] The objectives of this investigation were to 1) understand and quantify vertical shear in the horizontal plasma drift in the bottomside  $F$  region around sunset, 2) identify the mechanism producing the bottom-type scattering layers, and 3) assess the impact of the layers and shear flow on the overall stability of the postsunset equatorial  $F$  region.

[4] The investigation took place in August, 2004, during the NASA EQUIS II campaign on Kwajalein Atoll using a combination of sounding rockets and with the support of the Altair VHF/UHF coherent/incoherent scatter radar [Tsunoda *et al.*, 1979]. Two sets of launches took place on separate nights from the Roi Namur range. Each consisted of an instrumented payload launched north-westward and two chemical release payloads, one also launched north-westward, and the other launched to the northeast. The instrumented payloads measured plasma density, electron temperature, electron collision frequency, and electric field profiles to an altitude of about 450 km while the chemical release payloads afforded measurements of lower thermospheric neutral wind profiles at three locations though photographing and triangulation of chemiluminescent TMA trails [Larsen and Odom, 1997]. Radio beacons on the chemical release rockets along with the AFRL Digisonde were provided additional diagnostics.

### 2. Campaign Data

[5] The first experiment was conducted on August 7, 2004 following the appearance of  $F$  region coherent scatter in Altair radar scans at about 1930 SLT. Figure 1 shows UHF (422 MHz) radar data for three sequential scans occurring at 0840 UT, 0858 UT, and 0946 UT. Note that SLT  $\approx$  UT + 11 hr on Kwajalein. For these scans, the main beam of the radar was perpendicular to the geomagnetic field at  $F$  region altitudes. A combination of coherent and incoherent scatter was therefore detected. The incoherent scatter data have been processed so as to represent plasma density. Coherent echoes appear as intense patches superimposed on the incoherent scatter and signify the presence of nonthermal field-aligned plasma irregularities. Their widespread appearance signals the onset of ESF.

[6] The first two scans in Figure 1 show a bottom-type coherent scattering layer at 200–250 km altitude. The scans reveal that the layers are patchy, made up of periodically spaced regions of irregularities, separated in this case by about 150–200 km. Note that the same periodicity is seen in large-scale wave forming in the bottomside in the first two panels as well as in the radar plumes in the rightmost panel,

<sup>1</sup>Earth and Atmospheric Science, Cornell University, Ithaca, New York, USA.

<sup>2</sup>Physics and Astronomy, Clemson University, Clemson, South Carolina, USA.

<sup>3</sup>Electrical and Computer Engineering, Utah State University, Logan, Utah, USA.

<sup>4</sup>Electrical Engineering, Pennsylvania State University, University Park, Pennsylvania, USA.

<sup>5</sup>Jicamarca Radio Observatory, Instituto Geofísico del Perú Lima, Peru.

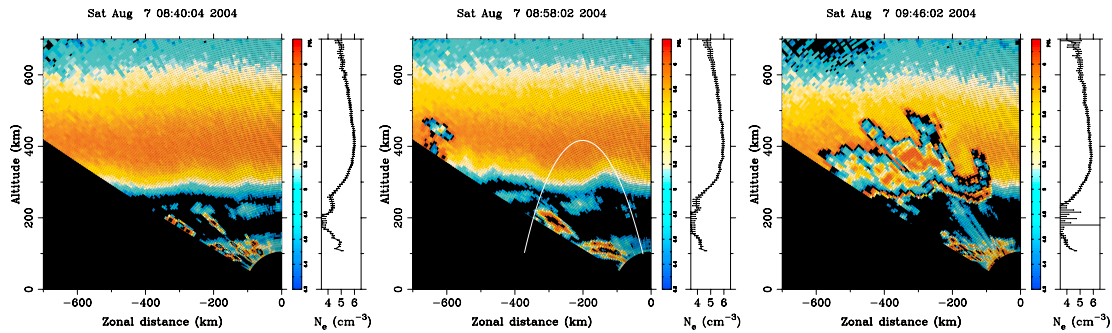


**Figure 1.** Altair radar scans prior to, during, and after the August 7 rocket flights. A combination of incoherent scatter (electron density) and coherent scatter (irregularity intensity) is shown. The white arc is the instrumented rocket trajectory. The rightmost panels depict electron density profiles at zenith.

when fully developed spread  $F$  was underway and distinct radar plumes separated by 150–200 km were visible.

[7] An instrumented rocket (29.036) was launched into the event at 0852:56 UT, followed by the two chemical release rockets. Rocket data are shown in Figure 2. The electron densities were derived by the Utah State University (USU) Swept Langmuir Probe, and the vector electric fields from the Penn State University (PSU) E-field experiment. In Figure 2, positive fields are eastward and upward and correspond, respectively, to upward and westward  $\mathbf{E} \times \mathbf{B}$  drifts. (Here, 1 mV/m corresponds to 33 m/s at 250 km altitude). The density profiles suggest a postsunset  $F$  region ionosphere with a steep bottomsides density gradient and a kink in the density at 350 km associated with the upwelling seen in the middle panel of Figure 1. The zonal electric field was small throughout the upleg except around 275 km where the vehicle entered the upwelling. Finally, the vertical electric field profile indicates strong shear flow, with the plasma moving eastward at up to 190 m/s above 250 km and westward at up to 50 m/s below 250 km. Values for the velocity shear (change in eastward plasma drift velocity with altitude) calculated from a low-pass filtered version of  $E_z$  approach +4 m/s/km in the bottomsides. A rapid eastward plasma jet at 275 km is co-located with the upwelling and presumably associated with the electric field of the growing large-scale wave.

[8] The payload also intercepted intermediate- and small-scale bottom-type plasma irregularities between 200–250 km altitude. The irregularities existed in the rarefied valley

region, where the density profile was flat, rather than the steep bottomsides, where Rayleigh-Taylor type instabilities are expected to occur. Moreover, the irregularities were confined to the westward-drifting strata below the shear node. Finally, the irregularities were anisotropic, with the vertical electric field components being significantly stronger than the zonal field components.

[9] The downleg data shown in Figure 3 are substantially similar to the upleg data. The steep bottomsides  $F$  region density gradient remains present. Strong shear flow continues, with the shear node falling at about 280 km. Weak plasma irregularities were grazed between 225–275 km altitude.

[10] The second set of rockets was launched on August 15 into the conditions depicted in Figure 4. A strong bottom-type scattering layer was forming directly overhead between about 225–300 km altitude. The layer was patchy rather than continuous and displayed regular, 30 km spacing between patches. Depletions and radar plumes ultimately formed exhibiting the same characteristic spatial periodicity as the bottom-type layer patches. A large-scale bottomsides undulation also emerged overhead during the experimental interval, seen most clearly near the rocket apogee in Figure 4. The instrumented rocket (29.037) launch occurred at 0821:53 UT, followed by two chemical release rockets. The arc in the middle panel of Figure 4 suggests that the instrumented rocket intercepted bottom-type layer patches on the upleg at 250–300 km altitude and on the downleg at somewhat lower altitude.

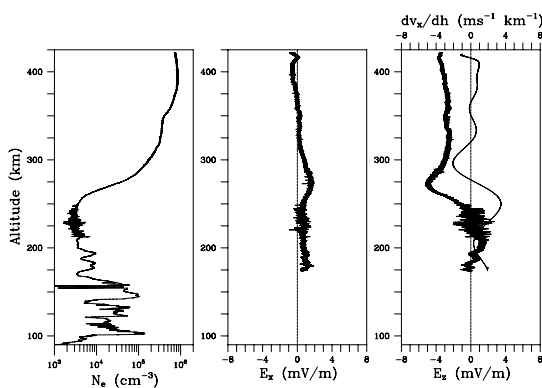


**Figure 2.** Upleg data from 29.036. Left: electron density. Center: zonal electric field. Right: vertical electric field. Right, light line: velocity shear.

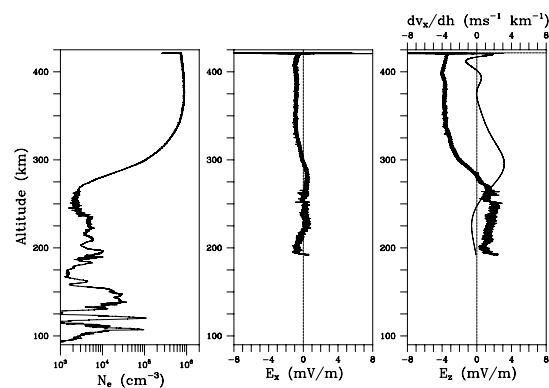


**Figure 3.** Downleg data from 29.036. Left: electron density. Center: zonal electric field. Right: vertical electric field. Right, light line: velocity shear.

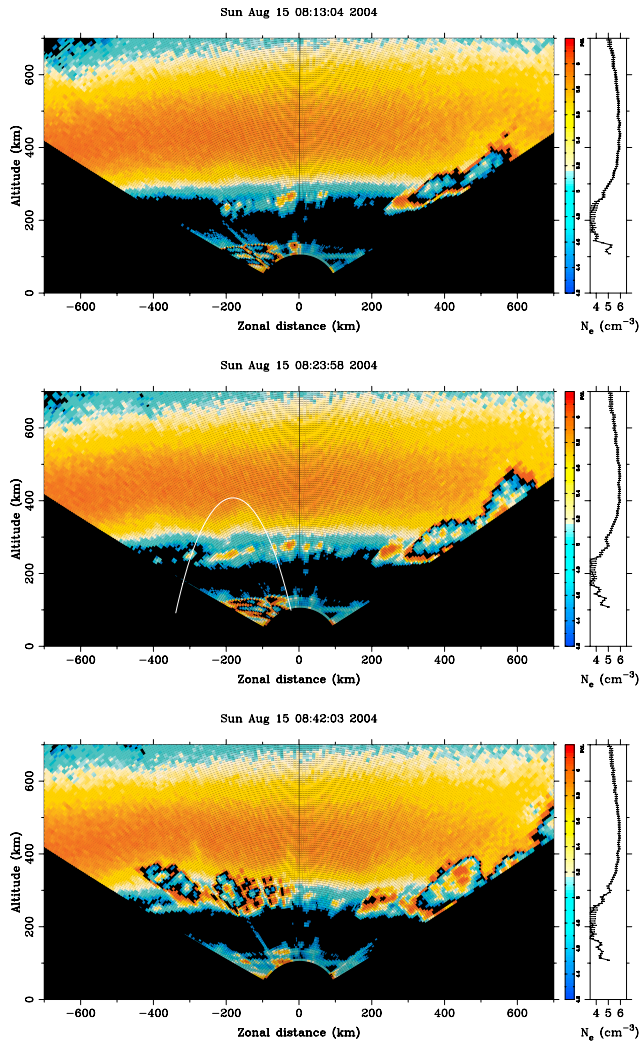


**Figure 4.** Altair radar scans prior to, during, and after the August 15 rocket flights. The white arc is the instrumented rocket trajectory. The rightmost panels depict electron density profiles at zenith.

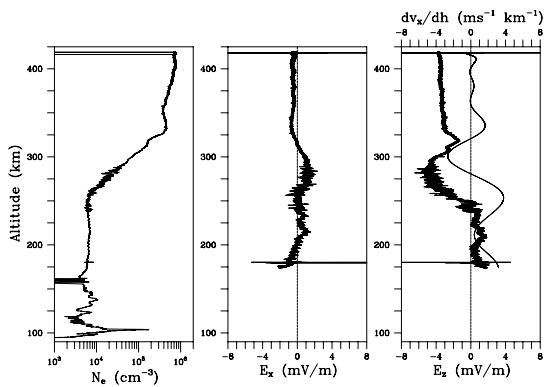


**Figure 5.** Upleg data from 29.037. Left: electron density. Center: zonal electric field. Right: vertical electric field. Right, light line: velocity shear.

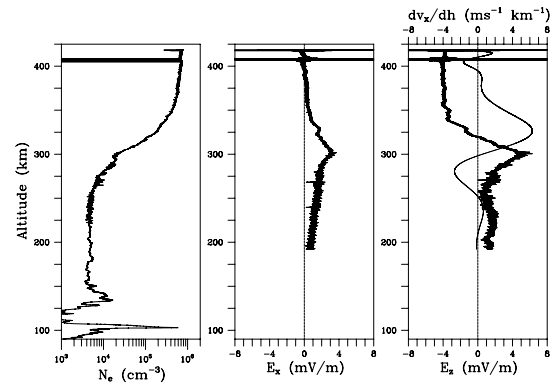


**Figure 6.** Downleg data from 29.037. Left: electron density. Center: zonal electric field. Right: vertical electric field. Right, light line: velocity shear.

[11] Upleg rocket measurements are shown in Figure 5, where irregularities are evident between about 240–300 km altitude. These irregularities were qualitatively different from the ones in the first experiment, existing both in the valley and the bottomside and demonstrating a greater degree of isotropy in their electric fields. Their relative RMS amplitude was smaller, but because the background density was an order of magnitude greater than before, the absolute density fluctuations were stronger. This is consistent with the detection of stronger coherent scatter from these layers. These irregularities moreover resided in a slowly ascending ionospheric layer that spanned the vertical shear node, occupying both eastward- and westward-drifting strata. The vertical electric field profile appears to be highly distorted, having jets moving eastward and westward with respect to the plasma at the  $F$  peak at altitudes just below and above 300 km respectively. We attribute this as well as the kinks in plasma density to the large-scale wave forming in the region and the emergence of ESF.

[12] Downleg data for the second instrumented rocket flight appear in Figure 6. These data are similar to those from August 7; the irregularities resided mainly in the valley region where the vertical density gradient was gradual and the plasma drifts were upward and westward. The irregularities were anisotropic, with larger RMS vertical electric field components than zonal. A strong westward jet in the plasma flow existed at about 300 km, a feature we associate with the growing large-scale bottomside undulation and imminent ESF. The velocity shear was as large as 6 m/s/km above the jet.

### 3. Summary and Analysis

[13] The vertical electric fields measured in situ confirm and quantify the strong shear flow and retrograde drifts in the postsunset bottomside  $F$  region inferred from radar observations by *Kudeki et al.* [1981] and *Tsunoda et al.* [1981]. The rocket experiments further show that bottom-type layers reside mainly in the valley region, below the altitudes where the vertical plasma density gradient is steepest and instead in the altitude range where the retrograde plasma drift is fastest. This, the fact that the vertical RMS perturbed electric fields in the layers are stronger than the zonal fields, and the widespread presence of zonal

plasma density gradients in the Altair data, support the theory of *Kudeki and Bhattacharyya* [1999] attributing the layers to wind-driven interchange instabilities.

[14] Moreover, coherent scatter data from the Altair radar confirm the observation that the bottom-type layers generally consist of patches regularly distributed in space as delineating the unstable western walls of an emerging large-scale wave. That the regular spacing of the patches was later replicated in the morphology of the depletions during full-blown ESF (Figures 1 and 4) argues that the layer patches are telltale of preconditioning or seed waves in the bottomside existing well in advance of ESF. Patchy bottom-type layers preceded the onset of ESF on every night that it occurred during our experiments on Kwajalein.

[15] *Hysell and Kudeki* [2004] analyzed whether shear flow could generate such large-scale seed waves. Following the analysis of *Keskinen et al.* [1988], they found a collisional branch of the electrostatic Kelvin Helmholtz instability that could operate in the bottomside in regions of retrograde plasma motion. The growth rate could compete with the Rayleigh Taylor instability but with potentially earlier onset. Nonlocal analysis predicted a maximum growth rate for  $kL \sim 1/2$ , where  $k$  is the horizontal wavenumber and  $L$  is the vertical scale length of the shear. Taking  $L \sim 15$  km on the basis of Figure 3 implies a preferred wavelength of about 200 km. An initial value analysis, meanwhile, suggested that the instability would exhibit a shorter dominant wavelength in its early stages, of the order of 30 km in simulation. The transient response of the instability could therefore account for the decakilometric large-scale waves in the postsunset ionosphere and that the steady-state response could account for the large scale ( $L \gtrsim 200$  km) waves. The instability is inherently nonlocal, and a growth rate cannot be evaluated on the basis of the local measurements presented here. A modeling effort dedicated to ascertaining the role of shear instability in the EQUIS II observations is underway.

[16] **Acknowledgments.** This work was supported by the National Aeronautics and Space Administration through grant no. NAG5-5380 to

Cornell University and grants NAG5-5373 and NAG5-5379 to Clemson University. The authors are indebted to the staffs of the Reagan Test Site on Kwajalein and of the Wallops Flight Facility who made this campaign possible and also to Erhan Kudeki and Robert Pfaff for many valuable discussions.

## References

- Hysell, D. L., and J. Burcham (1998), JULIA radar studies of equatorial spread  $F$ , *J. Geophys. Res.*, *103*, 29,155.
- Hysell, D. L., and E. Kudeki (2004), Collisional shear instability in the equatorial  $F$  region ionosphere, *J. Geophys. Res.*, *109*, A11301, doi:10.1029/2004JA010636.
- Hysell, D. L., J. Chun, and J. L. Chau (2004), Bottom-type scattering layers and equatorial spread  $F$ , *Ann. Geophys.*, *22*, 4061.
- Keskinen, M. J., H. G. Mitchell, J. A. Fedder, P. Satyanarayana, S. T. Zalesak, and J. D. Huba (1988), Nonlinear evolution of the Kelvin-Helmholtz instability in the high-latitude ionosphere, *J. Geophys. Res.*, *93*, 137.
- Kudeki, E., and S. Bhattacharyya (1999), Post-sunset vortex in equatorial  $F$ -region plasma drifts and implications for bottomside spread- $F$ , *J. Geophys. Res.*, *104*, 28,163.
- Kudeki, E., B. G. Fejer, D. T. Farley, and H. M. Ierick (1981), Interferometer studies of equatorial  $F$  region irregularities and drifts, *Geophys. Res. Lett.*, *8*, 377.
- Larsen, M. F., and C. D. Odom (1997), Observations of altitudinal and latitudinal  $E$ -region neutral wind gradients near sunset at the magnetic equator, *Geophys. Res. Lett.*, *24*, 1711.
- Tsunoda, R. T., M. J. Barons, J. Owen, and D. M. Towle (1979), Altair: An incoherent scatter radar for equatorial spread  $F$  studies, *Radio Sci.*, *14*, 1111.
- Tsunoda, R. T., R. C. Livingston, and C. L. Rino (1981), Evidence of a velocity shear in bulk plasma motion associated with the post-sunset rise of the equatorial  $F$  layer, *Geophys. Res. Lett.*, *8*, 807.
- Woodman, R. F., and C. La Hoz (1976), Radar observations of  $F$  region equatorial irregularities, *J. Geophys. Res.*, *81*, 5447.

A. Barjatya and C. M. Swenson, Department of Electrical and Computer Engineering, Utah State University, Logan, UT 84322, USA. (arohb@cc.usu.edu; charles.swenson@usu.edu)

J. L. Chau, M. F. Sarango, and R. F. Woodman, Jicamarca Radio Observatory, Instituto Geofísico del Perú, Lima 13, Peru. (jchau@jro.igp.gob.pe; msarango@jro.igp.gob.pe; ronw@geo.igp.gob.pe)

D. L. Hysell, Department of Earth and Atmospheric Sciences, Cornell University, Ithaca, NY 14853, USA. (daveh@geology.cornell.edu)

M. F. Larsen, Department of Physics and Astronomy, Clemson University, Clemson, SC 29634, USA. (mlarsen@hubcap.clemson.edu)

T. F. Wheeler, Department of Electrical Engineering, Pennsylvania State University, University Park, PA 16802, USA. (tfw1@psu.edu)